Superresolution Moiré Mapping of Particle Plasmon Modes

D. M. Koller, U. Hohenester, A. Hohenau, H. Ditlbacher, F. Reil, N. Galler, F. R. Aussenegg, A. Leitner, A. Trügler, and J. R. Krenn*

Institute of Physics and Erwin Schrödinger Institute for Nanoscale Research, Karl-Franzens-University, A-8010 Graz, Austria

(Received 16 December 2009; revised manuscript received 21 March 2010; published 9 April 2010)

The spontaneous emission rate of a fluorophore provides a direct probe of the photonic local density of states at the fluorophore position. Here we exploit this capability to map the plasmonic modes of gold nanoparticles by imaging the fluorescence intensity in combined regular arrays of identical gold and fluorophore-doped polymer nanoparticles. By varying the distance between gold and polymer particles across the array, the fluorophore emission generates an optical Moiré pattern corresponding to a magnified spatial map of the plasmonic mode, which can be directly imaged with an optical microscope. Our results are corroborated by supplementary theoretical model calculations.

DOI: 10.1103/PhysRevLett.104.143901 PACS numbers: 42.70.Qs, 73.20.Mf, 78.20.Ci, 78.67.Bf

Surface plasmons enable the nanoscale localization of light and provide an effective means to control the excitation and emission properties of quantum systems. These appealing properties have triggered a large variety of recent research in fields as diverse as data storage [1], quantum optics [2,3], optoelectronics [4,5], photovoltaics [6], and sensors [7]. With a demand for ever increasing miniaturization and integration densities for many of these applications, the spatially and spectroscopically resolved characterization of plasmonic nanostructures has to be improved as well. Recent developments in this direction include progress in near field scanning microscopy [8], two-photon luminescence based imaging [9] and spatially resolved electron energy loss spectroscopy [10,11].

In this Letter, we demonstrate a straightforward method to image plasmonic modes with subwavelength resolution, and spectral and polarization discrimination. To this end, we arrange identical copies of plasmonic gold nanoparticles in a 2D array, and superpose this pattern with a geometrically incommensurable 2D array of dye doped polymer nanoparticles. The dye emission is spectrally tuned to the plasmonic resonance and thus serves as a sensitive probe of the plasmonic mode density [12]. As the distance between gold and polymer particles varies across the array, a microscale Moiré pattern is generated by the dye emission that corresponds to a magnified spatial map of the plasmonic mode.

Metal structures sustaining surface plasmons can substantially alter the excitation and emission rates of a nearby quantum system as, e.g., a fluorophore [13,14]. While excitation rates can be increased by the strong local plasmonic fields, the molecular emission rate is boosted in response to the high plasmonic local density of states (LDOS) according to Fermi's golden rule [15]. It has been shown recently that fluorophores with a large Stokes shift allow us to access the emission channel modification only [12], thereby enabling direct measurements of the plasmonic LDOS. Here, we apply this approach to the high-resolution mapping of the plasmonic modes of lithographically tailored gold nanoparticles with resonance wavelengths in the red spectral range [black line in Fig. 1(a)].

Square gold nanoparticles (side length 100 nm, height 50 nm) were fabricated over an area of 100 μm $\times$ 100 μm, arranged in a regular square array with a grating constant of $G = 400$ nm on indium-tin-oxide covered glass substrates by an electron beam lithography lift-off process relying on the positive resist poly(methyl methacrylate). We found the gold nanoparticles to be geometrically virtually identical throughout the array [upper left image in Fig. 1(b)]. Individual features in particle geometry deviating from the mean shape can amount to ± 3 nm, limiting the achievable spatial resolution, while variations of the plasmonic resonance are negligible. As the fluorophore we chose a platinum porphyrin (PtTFPP) [16] with an absorption band in the blue spectral range and an emission band centered at a wavelength of 650 nm. In this case the plasmonic influence on the absorption rate is negligible [12]. PtTFPP was mixed at a concentration of 49.5 g/l into the negative tone resist SU-8-3010 (MicroChem Corp.) which was diluted before with SU8-2000 thinner (MicroChem Corp.) at a ratio of 1:20. This concentration was found to yield homogeneously dispersed molecules with easily detectable fluorescence signal levels which are not strongly affected upon electron irradiation. Electron beam exposure of a 60 nm thick PtTFPP doped SU8 film deposited by spin coating on indium-tin-oxide covered glass substrates yielded nanoparticles with a diameter of 40 nm and a height of 60 nm, containing about 2000 PtTFPP molecules each. Again, the particles were arranged in a square array with $G = 400$ nm over an area of 100 μm $\times$ 100 μm [upper right image in Fig. 1(b)]. A photoluminescence spectrum of this array is shown by the red line in Fig. 1(a).

By combining both lithography schemes to an aligned two-step writing process, we fabricated heterogeneous arrays of gold and SU8/PtTFPP nanoparticles, as shown in the lower row of Fig. 1(b). SU8/PtTFPP particles posi-

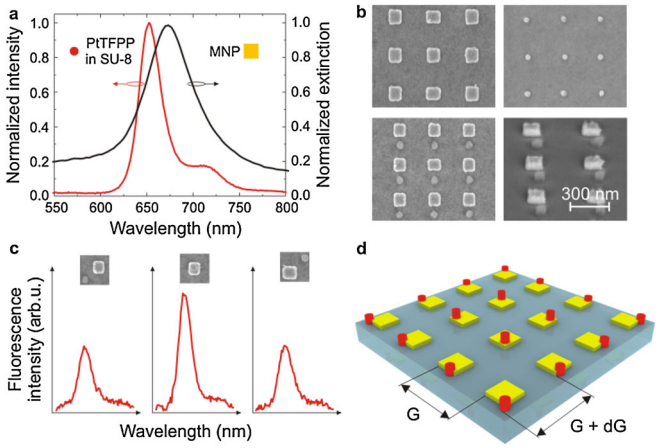

FIG. 1 (color online). Principles of fluorescence Moiré mapping of gold nanoparticles. (a) Normalized plasmonic extinction (black curve) and photoluminescence spectra (red curve) of gold and SU8/PtTFPP nanoparticle arrays, respectively. (b) Scanning electron micrographs of (upper row) arrays of gold and SU8/PtTFPP nanoparticles and (lower row) a combined array of both nanoparticle types. (c) Photoluminescence spectra acquired from heterogeneous arrays of gold and SU8/PtTFPP nanoparticles. The relative mutual position of the nanoparticles within the array is shown in the insets for one particle pair. (d) Schematic sketch of distance variations of both types of nanoparticles within the combined arrays used for Moiré imaging, due to two different grating constants G and $G + dG$.

tioned directly on gold particles showed about 2 times larger volumes as compared to particles sitting directly on the substrate which is most likely due to increased electron backscattering during the lithographic exposure process. We note that quenching in the case of SU8 particles in direct contact with a gold particle does not play a major role as only a few molecules are within quenching distance [13] due to the height of the SU8 particle. The measured integral fluorescence intensity from the heterogeneous arrays depends on the mutual distance of gold and SU8/PtTFPP nanoparticles, thus giving a measure of the LDOS at the position of the molecules [Fig. 1(c)]. While the presence of the SU8 particle in principle causes a modification of the dielectric environment of the gold particle, measurements on arrays with different mutual distances of both types of particles show that no significant spectral modification of the plasmonic band takes place.

We next increased the grating constant for the SU8/PtTFPP array by $dG = 2$ nm to 402 nm, while maintaining $G = 400$ nm for the gold particle array. The distance between SU8/PtTFPP and gold nanoparticles forming neighboring pairs is thus shifted by dG when moving from one pair to the next. The fluorescence emission intensity changes accordingly, spatially sampling the plasmonic LDOS [Fig. 1(d)]. Consequently, the fluorescence intensity distribution within the array as directly observable with a microscope is an image representing the LDOS of the (virtually identical) gold particles, with a magnification factor of $G/dG = 200$. The achievable spatial resolution is determined by the smallest possible step size in the lithographic process, and is not limited by diffraction.

An exemplary fluorescence image of a square gold nanoparticle under unpolarized illumination is shown in Fig. 2(a). The variation of the mutual distance between gold and SU8/PtTFPP nanoparticles is illustrated in the insets for five positions within the array. We observe a well-defined square pattern in the fluorescence image, corresponding to the particle geometry. The ratio of the full-width-at-half-maximum of the fluorescence pattern [as defined in the cross cut in Fig. 2(b)] and the particle size is 210. While a comparison of the dimensions of the geometrical particle size and the plasmonic mode pattern is in principle meaningless, the found value is nevertheless close to the magnification value of 200, as defined above, due to the strong localization of the plasmonic field to the particle surface. The curvature of the particle corners of about 5 nm is very well reproduced in the image, emphasizing nanoscale spatial resolution.

A key advantage of our method is the direct access to polarization-dependent and spectroscopic information by simply introducing a polarizer and spectral filters into the optical detection branch. Therefore, additional filters for spectral selectivity (band pass 650 ± 10 nm, 670 ± 10 nm and long pass ≥ 720 nm), and a polarizer in front of the camera were used. Figure 3(a) shows a series of images of the square gold nanoparticle as in Fig. 2(a) but with both polarized and spectrally filtered detection, indicated to the left and on top of the image, respectively. Depending on polarization the mode pattern appears rotated by 90°, as expected for a dipolar excitation. The spectrally filtered images reveal subtle changes when moving the spectral window over the plasmonic resonance at 670 nm [Fig. 1(a)]. Both to the short-wavelength side of the resonance (band-pass filter 650 ± 10 nm) and on-resonance

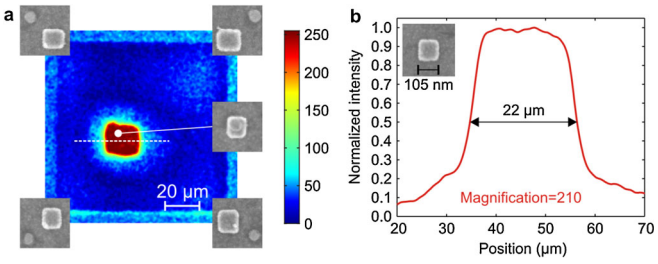

FIG. 2 (color online). Fluorescence Moiré mapping of a gold nanoparticle. (a) Image of a square gold nanoparticle. Unpolarized excitation at wavelengths of 365 ± 20 nm and detection through a high-pass filter with a cutoff wavelength of 515 nm were applied using a 20x, numerical aperture = 0.5 microscope objective. The scanning electron micrographs in the insets illustrate the variable distance between gold and SU8/PtTFPP nanoparticles, according to their position within the array. (b) Cross cut along the dashed line in (a) revealing a ratio of Moiré image size and geometrical particle size (inset) of 210.

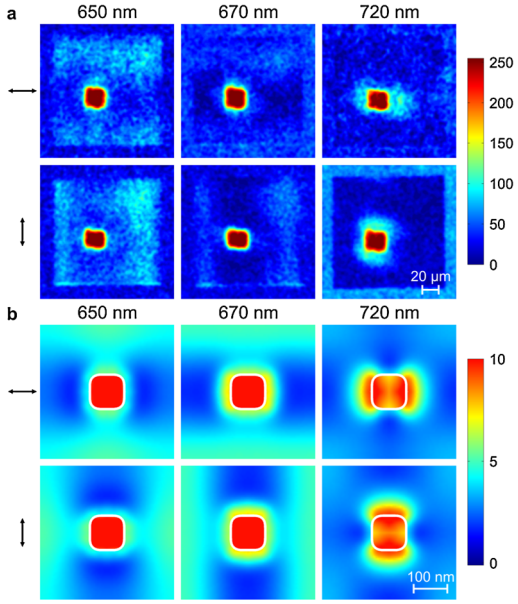

FIG. 3 (color online). Polarization and wavelength dependence of the plasmon mode of a square gold nanoparticle. Polarization directions and wavelength ranges are given to the left and on top, respectively. (a) Experimental images for (upper row) horizontal and (lower row) vertical polarization and spectral ranges (left to right) 650 ± 10 nm, 670 ± 10 nm and ≥ 720 nm. (b) BEM simulations for the polarization directions indicated to the left and for discrete wavelengths of (from left to right) 650, 670, and 720 nm.

(band-pass filter 670 ± 10 nm) the plasmonic mode appears strongly localized to the particle while on the long-wavelength side (long-pass filter ≥ 720 nm) the dipolar mode pattern extends further away from the particle. In addition, we observe bright and dark areas in between the nanoparticles corresponding to areas of enhanced and suppressed LDOS, to be discussed below. Areas of increased LDOS are particularly strong for the wavelength band 650 ± 10 nm, according to a radiating grating order at near-grazing angles [17]. We note that the intensity levels in the images are normalized to optimum contrast as molecular bleaching taking place during image acquisition (corresponding to about 5% intensity decrease) makes the comparison of absolute signal levels impossible.

For closer analysis of the experimental data we performed simulations based on the boundary element method (BEM) [18,19], which does not introduce any fitting parameters. The dielectric function of gold was extracted from optical data [20]. As the presence of a substrate was not taken into account in the calculations we assumed a homogeneous medium with a refractive index of 1.5. The geometry of the modeled gold nanoparticles ($100 \times 100 \times 50$ nm^3 for the square particles and $100 \times 300 \times 50$ nm^3 for the nanorods) were chosen to match the measured extinction spectra. To account for the regular particle arrangement we simulate an ensemble of four gold nanoparticles arranged according to the experimental conditions, i.e., $G = 400$ nm. We model the molecules as dipole resonators, with moment $\mathbf{d}$, which are situated at positions $\mathbf{r}$. To account for the off-resonant excitation, we assume that the molecule is initially excited and subsequently decays, either through electromagnetic coupling or via intramolecular channels. The electromagnetic decay rate $\gamma_{\mathrm{em}}(\mathbf{d}, \mathbf{r}, \omega)$ at a given photon energy $\hbar\omega$ is obtained from the imaginary part of the dyadic Green function [15], and the intramolecular decay rate γ_{mol} is related to the quantum yield of the isolated molecule, which we estimate to be about 10% [21]. With $\gamma_{\mathrm{rad}}^{\Omega,\ell}$ denoting the differential cross section for light emission into a sphere segment Ω, which corresponds to the experimental conditions, and ℓ being the polarization, we can express the measured luminescence intensity, governed by the plasmonic LDOS, as

$$I_{\mathrm{lum}}^{\Omega,\ell}(\mathbf{R_0}, \omega) \propto \left\langle \frac{\gamma_{\mathrm{rad}}^{\Omega,\ell}(\mathbf{d}, \mathbf{r}, \omega)}{\gamma_{\mathrm{em}}(\mathbf{d}, \mathbf{r}, \omega) + \gamma_{\mathrm{mol}}} \right\rangle. \quad (1)$$

This quantity describes the probability that an excited molecule emits a photon into the direction of the photodetector. The brackets denote an ensemble average over the dipole orientations and positions $\mathbf{r}$ within the SU8 nanoparticle, centered at $\mathbf{R_0}$. We assume a homogeneous distribution of randomly oriented dipole moments within a volume corresponding to the SU8 nanoparticle. The larger volume of the SU8/PtTFPP particles on top of the gold particles has been taken into account accordingly.

Figure 3(b) shows maps calculated with Eq. (1) which directly correspond to the experimental images in Fig. 3(a). We emphasize that the simulation shows a single particle while in the experiment a magnified image including many nanoparticles is observed. From the comparison of the according images in Figs. 3(a) and 3(b) the agreement of experiment and simulation is evident, which we take as direct proof of the LDOS imaging properties of our system. In particular, the evolution of the spatial profile of the LDOS pattern as a function of observation wavelength is well reproduced. We found that the dark spots in between the particles occur at the positions where the electric field of the induced surface plasmon interferes destructively with the driving dipole of the molecule. Because of the phase difference between driving dipole and driven molecule, the composite system has a *smaller* effective dipole, thus corresponding to a smaller LDOS.

Next, we investigate gold nanorods with a cross section diameter and length of 100 and 300 nm, respectively, and a height of 50 nm, arranged in a square pattern with $G = 400$ nm. The dipolar resonances for excitation light polarizations along the short and long nanorod axes lie at a wavelength of 660 nm and in the infrared spectral range, respectively. The relative positions of nanorods and SU8/PtTFPP nanoparticles throughout the array were chosen such that two entire and part of two further nanorods appear in the images. Figure 4(a) shows the experimental images, for experimental parameters as in Fig. 3. For polarization along the short nanorod axis we again find

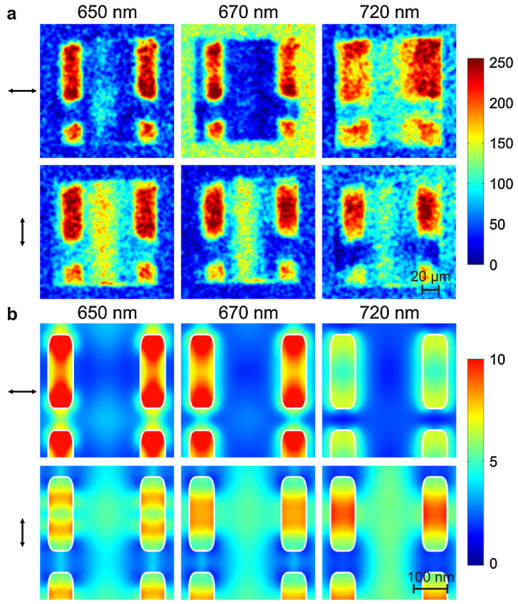

FIG. 4 (color online). Polarization and wavelength dependence of the plasmon mode of a gold nanorod. (a) Experimental images as in Fig. 3, but for a gold nanorod with 300 nm length, 100 nm width, and 50 nm height. Corresponding BEM simulations (compare Fig. 3).

strongly localized mode patterns for the short-wavelength side of the resonance and on-resonance. The corresponding calculations in Fig. 4(b) reveal these patterns as due to excitations of a dipolar plasmonic mode along the short axis of the nanorod. For the off-resonant case (wavelengths $\geq$720 nm) less confined fields are observed, again corresponding to the simulation. Choosing the polarization direction along the nanorod axis we find that the fluorescence signal becomes more confined to the center of the nanorod when increasing the observation wavelengths. The comparison with the simulations in Fig. 4(b) reveals the likely explanation for this effect. For wavelengths $\geq$720 nm a nonresonant excitation of the dipolar resonance (in the infrared spectral range) dominates, giving rise to a rather localized mode pattern. For a wavelength of 650 nm, however, the quadrupolar mode prevails, corresponding to a spatially more extended mode. Again, the fluorescence maxima in between the nanorods can be explained due to the grating effect.

The superresolution access to plasmonic modes by fluorescence Moiré mapping as discussed here can in principle be extended to any nano-optical system. While SU8/PtTFPP nanoparticles have been found to be a particularly stable probe for the LDOS, probing other wavelength ranges on the basis of different fluorophores is straightforward. The challenge of well-controlled pattern fabrication could possibly be met by nanoimprinting based processes. Besides LDOS mapping and nanoparticle or quantum emitter studies, such systems could be useful for applications in sensors or wavelength and polarization encoded security features.

The Graz Advanced School of Science (GASS) of NAWI Graz is acknowledged for financial support.

*joachim.krenn@uni-graz.at

[1] P. Zijlstra, J. W. M. Chon, and M. Gu, Nature (London) **459**, 410 (2009).
[2] A. V. Akimov, A. Mukherjee, C. L. Yu, D. E. Chang, A. S. Zibrov, P. R. Hemmer, H. Park, and M. D. Lukin, Nature (London) **450**, 402 (2007).
[3] R. Kolesov, B. Grotz, G. Balasubramanian, R. J. Stöhr, A. A. L. Nicolet, P. R. Hemmer, F. Jelezko, and J. Wachtrup, Nature Phys. **5**, 470 (2009).
[4] D. M. Koller, A. Hohenau, H. Ditlbacher, N. Galler, F. Reil, F. R. Aussenegg, A. Leitner, E. J. W. List, and J. R. Krenn, Nat. Photon. **2**, 684 (2008).
[5] A. L. Falk, F. H. L. Koppens, C. L. Yu, K. Kang, N. de Leon Snapp, A. V. Akimov, M.-H. Jo, M. D. Lukin, and H. Park, Nature Phys. **5**, 475 (2009).
[6] V. E. Ferry, L. A. Sweatlock, D. Pacifici, and H. A. Atwater, Nano Lett. **8**, 4391 (2008).
[7] J. N. Anker, W. P. Hall, O. Lyandres, N. C. Shah, J. Zhao, and R. P. van Duyne, Nature Mater. **7**, 442 (2008).
[8] M. Schnell, A. Garcia-Etxarri, A. J. Huber, K. Crozier, J. Aizpurua, and R. Hillenbrand, Nat. Photon. **3**, 287 (2009).
[9] P. Ghenuche, S. Cherukulappurath, T. H. Taminiau, N. F. van Hulst, and R. Quidant, Phys. Rev. Lett. **101**, 116805 (2008).
[10] J. Nelayah, M. Kociak, O. Stephan, F. J. G. de Abajo, M. Tence, L. Henrard, D. Taverna, I. Pastoriza-Santos, L. M. Liz-Marzan, and C. Colliex, Nature Phys. **3**, 348 (2007).
[11] B. Schaffer, U. Hohenester, A. Trügler, and F. Hofer, Phys. Rev. B **79**, 041401(R) (2009).
[12] S. Gerber, F. Reil, U. Hohenester, T. Schlagenhaufen, and A. Leitner, Phys. Rev. B **75**, 073404 (2007).
[13] P. Anger, P. Bharadwaj, and L. Novotny, Phys. Rev. Lett. **96**, 113002 (2006).
[14] S. Kühn, U. Hakanson, L. Rogobete, and V. Sandoghdar, Phys. Rev. Lett. **97**, 017402 (2006).
[15] L. Novotny and B. Hecht, *Principles of Nano-Optics* (Cambridge University Press, Cambridge, England, 2006).
[16] Platinum(II)-5,10,15,20-tetrakis-(2,3,4,5,6-pentafluorphenyl)-porphyrin.
[17] B. Lamprecht, G. Schider, R. T. Lechner, H. Ditlbacher, J. R. Krenn, A. Leitner, and F. R. Aussenegg, Phys. Rev. Lett. **84**, 4721 (2000).
[18] F. J. Garcia de Abajo and A. Howie, Phys. Rev. B **65**, 115418 (2002).
[19] U. Hohenester and A. Trügler, IEEE J. Sel. Top. Quantum Electron. **14**, 1430 (2008).
[20] P. B. Johnson and R. W. Christy, Phys. Rev. B **6**, 4370 (1972).
[21] M. I. J. Stich, S. Nagl, O. Wolfbeis, U. Henne, and M. Schaeferling, Adv. Funct. Mater. **18**, 1399 (2008).